

BL11XU QST Quantum Dynamics I

1. Introduction

BL11XU is an in-vacuum undulator beamline operated by the National Institutes for Quantum and Radiological Science and Technology (QST). It is designed to provide scientists and engineers with a wide range of options on advanced synchrotron radiation and quantum functional material research. In this beamline, switchable Si(111) and Si(311) double-crystal monochromators cooled by liquid nitrogen are installed in the optical hutch. Highly brilliant and directional synchrotron X-rays are available in the energy range of 6–70 keV. There are three experimental hutches; each one contains specialized measurement instruments for studies using Mössbauer spectroscopy (EH1), inelastic X-ray scattering and X-ray magnetic circularly polarized emission (EH2), and surface X-ray diffraction (EH3).

2. Mössbauer spectroscopy

The ^{57}Fe probe layer method acquires a layer-by-layer Mössbauer spectrum by carefully constructing a film made of ^{56}Fe (non-resonant isotope) and introducing a monolayer (ML) of ^{57}Fe (resonant isotope) at the desired depth from the surface. Recently, a high-brilliance synchrotron radiation source (SMS) has greatly improved the ^{57}Fe probe layer method [1,2]. This method can rapidly measure the absorption spectrum of the ^{57}Fe probe for one monolayer (ML) embedded in the film surface using the total reflection of ^{57}Fe Mössbauer γ -rays filtered from synchrotron radiation.

To realize a more advanced ^{57}Fe probe layer

method, simultaneous measurements of γ -rays and the conversion electron Mössbauer spectra of an isotope-substituted Fe/Cr multi-layer film under total reflection conditions were performed using a ^{57}Fe SMS [3]. A Cr/Fe multi-layer film (Cr (1 nm)/ ^{56}Fe (99.4%, 2 nm)/ ^{57}Fe (95%, 0.2 nm)/ ^{56}Fe (99.4%, 8 nm)/Cr (1 nm)/MgO(001) was prepared by molecular beam epitaxy. Then experiments were performed at BL11XU using π -polarized 14.4 keV Mössbauer γ -rays with a 15.4 neV bandwidth produced by a SMS (Fig. 1). An external field of 800 Oe was applied parallel to the beam direction to magnetize the film, and the π -polarized γ -rays interacted with the four nuclear transitions of $\Delta m = \pm 1$. The absorption spectra were measured by collecting the totally reflected γ -rays and scattered

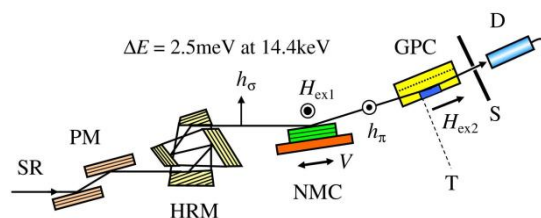


Fig. 1. Experimental setup. SR: Synchrotron radiation from the undulator of BL11XU; PM: premonochromator, Si 111 reflections; HRM: high-energy-resolution monochromator, nested-type channel-cut Si 511×975 reflections; NMC: nuclear monochromator crystal, $^{57}\text{FeBO}_3$ 111 near the Néel temperate; H_{ex1} : Magnetic field of 130 Oe; GPC: gas-flow proportional counter; H_{ex2} : magnetic field of 800 Oe; S: Slit, 1.0 mm \times 4.0 mm; D: NaI(Tl) detector; T: target sample.

conversion electrons using a NaI(Tl) scintillation detector and gas-flow proportional counter, respectively.

Figure 2 shows the γ -ray and conversion electron spectra of the Cr/Fe film with a ^{57}Fe probe ML at different incidence angles of 0.15° and 0.3° . Here, the contribution of the nuclear and electronic scatterings to the total reflection was reversed near the critical angle of electronic scattering, $\theta_c \sim 0.22^\circ$ for the Fe film [1].

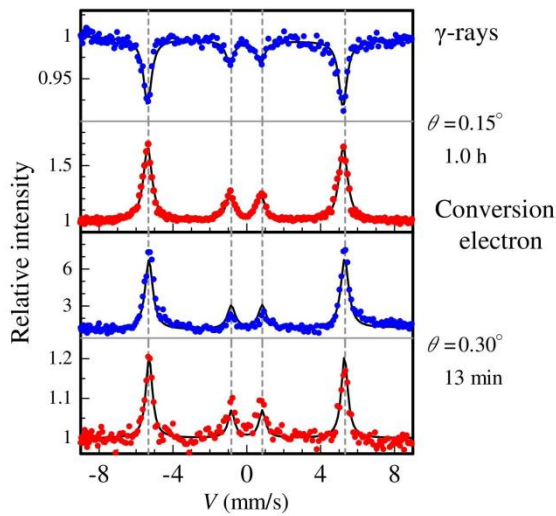


Fig. 2. Mössbauer spectra of the magnetized Fe/Cr film containing the ^{57}Fe ML resonant atoms at different grazing angles obtained using the totally reflected γ -rays (upper panel) and conversion electrons (lower panel). Four dashed lines on the velocity axis indicate the hyperfine resonance energies of α -Fe at 300 K. Solid lines are the fitting curves.

At $\theta_{\text{in}} = 0.15^\circ (< \theta_c)$, the contribution of the electronic scattering was dominant. Thus, the γ -ray and conversion electron spectra were normal absorption and scattering Mössbauer spectra, respectively. By contrast, at $\theta_{\text{in}} = 0.3^\circ (> \theta_c)$, the

γ -ray spectrum consisted of upward peaks because the total reflection was dominated by the nuclear resonant scattering from the ^{57}Fe probe ML, while that of the electronic scattering was suppressed (i.e., pure nuclear total reflection (PNTR)). It should be noted that the observed PNTR spectrum exhibited a high signal-to-noise ratio and the spectrum of the ^{57}Fe probe ML was acquired in a short time of 13 min (Fig. 2, lower panel, blue line). The quality of the PNTR spectrum was much higher than that of the conversion electron spectrum, indicating that the ^{57}Fe probe layer method with PNTR is efficient for thin-film studies. The excellent performance opens the door for further studies on surface and interface magnetism in advanced magnetic and spintronic materials and devices.

3. Inelastic X-ray scattering

EH2 contains an inelastic scattering spectrometer for hard X-rays. Resonant inelastic X-ray scattering (RIXS) at the K -edge of the $3d$ transition metal and the L -edge of $5d$ transition metal is one of the main activities. RIXS provides element-selective and momentum-resolved electronic excitation spectra. Recently, $5d$ transition-metal compounds have received attention in the search for novel electronic states generated by the interplay between on-site Coulomb repulsion and strong spin-orbit coupling. In the past few years, monochromators and analyzers for the L_3 -edge of some $5d$ transition-metal elements have been introduced and spin-orbit-entangled $5d$ -electronic states have been studied through the observation of dd excitations using $5d$ transition-metal L_3 -edge RIXS.

In Rb_2TaCl_6 , Ta^{4+} ion of the $5d^1$ state is surrounded by a spatially separated regular octahedron of $(\text{Cl}^-)_6$. That is, the $5d$ electron is situated in an ideal environment for the spin–orbit entangled state of $J_{\text{eff}} = 3/2$ without lattice distortions. In fact, the dd excitations of Rb_2TaCl_6 form a single peak with a resolution-limited width^[4] and the peak is assigned to a transition from the degenerated $J_{\text{eff}} = 3/2$ to $J_{\text{eff}} = 1/2$ states. On the other hand, Ir^{4+} ion ($5d^5$ state) in the pyrochlore iridates $A_2\text{Ir}_2\text{O}_7$ ($A =$ trivalent ion) occupies the $(\text{O}^{2-})_6$ -octahedron with a trigonal distortion. The distortion lifts the degeneracy of the $J_{\text{eff}} = 3/2$ states and rearranges the spin–orbit entangled states. As a result, the dd excitations split into two peaks. $\text{In}_2\text{Ir}_2\text{O}_7$ has the largest distortion in the pyrochlore iridates. Unexpectedly, a RIXS study^[5] demonstrated that peak separation of the dd excitations was small in $\text{In}_2\text{Ir}_2\text{O}_7$ compared with other pyrochlore iridates. The reduced intersite hopping due to the distortion and covalent character of the In–O bond plays a predominant role in the $5d$ -electronic states of $\text{In}_2\text{Ir}_2\text{O}_7$ rather than local distortion.

The spectrometer has also been used for X-ray emission spectroscopy. The $K\beta$ emission of $3d$ transition metal is correlated with the magnitude of the local magnetic moment. Combined with observations of collective magnetic excitations using RIXS and the Fe L_3 -edge, the coexistence of localized and itinerant nature of electrons in the iron pnictide superconductors $\text{BaFe}_2(\text{As}_{1-x}\text{P}_x)_2$ was identified^[6].

4. X-ray magnetic circularly polarized emission

X-ray magnetic circularly polarized emission (XMCPE) is a phenomenon in which characteristic

X-rays emitted from a magnetized sample are circularly polarized. In FY2017, XMCPE was reported as a new magneto-optical effect in the X-ray region^[7]. An advantage of XMCPE is the large flipping ratio ($>20\%$) in the hard X-ray region for $3d$ transition metal elements. This feature is well suited for observations of magnetic microstructures well below the sample surface. In FY2018, the development of a bulk-sensitive magnetic microscope utilizing XMCPE began in BL11XU. First, an XMCPE microscope was constructed (Fig. 3), and it was used to observe the magnetic domains in an electrical steel sheet with an incident X-ray energy of 17.3 keV. The crucial elements are (i) the focusing optics, (ii) collimating optics, and (iii) circular polarization analyzer. The focusing optics focuses incident X-rays onto a sample. Two compound refractive lenses were equipped. The focus size of each lens was about 10 μm . The collimating optics transforms a divergent fluorescence X-ray beam into a well-collimated one. We employed a laterally graded multilayer Montel mirror. The acceptance angle of the mirror is $21 \text{ mrad} \times 21 \text{ mrad}$, and the multilayer period is tuned for 6.4 keV (Fe $K\alpha$ emission). The circular polarization analyzer consists of a phase plate (diamond 220) and a linear polarization analyzer (Ge 400). The diamond phase plate converts circular polarization to linear polarization. Then the converted linear polarization is evaluated by the linear polarization analyzer. Accordingly, the obtained linear polarization agrees with the initial circular polarization.

In FY2019, the angular divergence of the collimated X-ray beam, which is an important quantity that characterizes the performance of the XMCPE microscope, was evaluated. Using a

double-crystal analyzer with two Si (400) crystals in the ++ arrangement, an angular divergence of 120 μrad was obtained. This divergence was slightly wider than the designed value of 100 μrad . Next, a higher incident X-ray energy of 26 keV was used to obtain magnetic information much deeper inside a sample. The magnetic domains of a grain-oriented electrical steel sheet at 26 keV and 17.3 keV were observed with step sizes 30 $\mu\text{m} \times 30 \mu\text{m}$ and 10 $\mu\text{m} \times 10 \mu\text{m}$. The basic stripe domains and several lancet domains were observed. Additionally, the exit-angle dependence was measured at the incident X-ray energy of 26 keV.

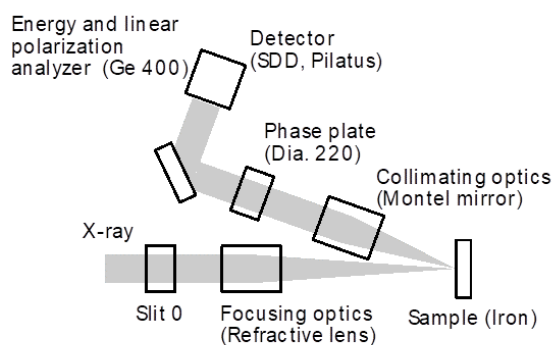


Fig. 3. Schematic of the XMCPE microscope in BL11XU.

5. Surface X-ray diffraction

EH3 is equipped with a surface X-ray diffractometer connected with a molecular beam epitaxy (MBE) chamber [8,9]. This instrument is designed for *in situ* studies on III–V group semiconductor surfaces, especially surface crystallography under MBE conditions and growth dynamics of multilayer and nanostructures. III–V group semiconductors are nitrides such as GaN and InN and arsenides such as GaAs and InAs. These semiconductors are grown by exchanging two types of MBE chambers. The nitride-MBE

chamber with an upgraded vacuum pumping system enhances the flow rate of nitrogen gas, realizing a 75% increase in the growth rate. This enhanced flow rate facilitates *in situ* structural analysis of the nitrides under high growth rate conditions as well as reduces the crystal growth time.

Our recent activity on nitrides focuses on the evolution of lattice strain and the indium composition at the nitride heterointerfaces [10]. *In situ* X-ray diffraction reciprocal space mapping (*in situ* RSM) measurements were performed for the radio frequency (RF) plasma-assisted MBE growth of InGaN on GaN and InN layers, which were grown by RF-MBE on commercialized GaN/c-sapphire templates. Both lattice relaxation and compositional pulling occurred during the initial growth stage, reducing the strain of InGaN on GaN and InN. Different initial growth behaviors of InGaN on GaN and InN were also observed from the results of the evolution of InGaN-integrated peak intensities.

Takaya Mitsui*¹, Kenji Ishii*¹, Toshiya Inami*¹, and Takuo Sasaki*²

*¹ Magnetism Research Group, National Institutes for Quantum and Radiological Science and Technology

*² Coherent X-ray Research Group, National Institutes for Quantum and Radiological Science and Technology

References:

- [1] T. Mitsui et al. (2012). *J. Synchrotron Radiat.*, 19, 198.
- [2] T. Mitsui et al. (2016). *J. Phys. Soc. Jpn.*, 85, 063601.

- [3] T. Mitsui et al. (2020). *J. Phys. Soc. Jpn.*, 89, 054707.
- [4] H. Ishikawa et al. (2019). *Phys. Rev. B*, 100, 045142.
- [5] A. Krajewska et al. (2020). *Phys. Rev. B*, 101, 121101(R).
- [6] J. Pelliciani et al. (2019). *Commun. Phys.*, 2, 139.
- [7] T. Inami. (2017). *Phys. Rev. Lett.*, 119, 137203.
- [8] M. Takahasi. (2013). *J. Phys. Soc. Jpn.*, 82, 021011.
- [9] T. Sasaki et al. (2016). *Jpn. J. Appl. Phys.* 55, 05FB05.
- [10] T. Yamaguchi et al. (2019). *Crystals*, 9, 631.